

# **The Origin and Evolution of Deep Plasmaspheric Notches**

D. L. Gallagher

NASA Marshall Space Flight Center

M. L. Adrian

NASA Goddard Space Flight Center

M. W. Liemohn

University of Michigan

Submitted to J. Geophys. Res., 2004

## **Abstract**

Deep plasmaspheric notches can extend over more than 2 RE in radial distance and 3 hours MLT in the magnetic equatorial plane. They appear to be among the largest evacuated features in the exterior plasmaspheric boundary. They can last for days and exhibit varying structure. It appears that low-density channels resulting from the entrainment of the plasmaspheric convection plume during storm-time recovery share the same origin as notches. Notches rather than channels result from differences in storm-time conditions. Strong convection tends to result in low-density channels, while weaker convection and limited erosion results in notches. Eighteen events in 2000 have been analyzed. Among these events, notches were found to drift as slowly as 72% of corotation. In only one case was a notch found to drift at the corotation rate within measurement error. On average, notches drift at about 21.5 hours per day or 90% of the corotational rate. Notches also sometimes exhibit an interior structure that appears as an extended prominence of dense plasma, which forms a W-like feature in IMAGE/EUV images when viewed from Earth-center. Modeling suggests such features may be caused by small-scale potential structures that result from the localized injection of ring current plasma. Plasma filling rates during recovery and drainage during a minor storm are reported.

## Introduction

The plasmasphere, a relatively dense toroidal region of cold plasma surrounding the Earth, has been studied for many years [see *Lemaire and Gringauz, 1998*] and is thought to play an important role in energetic particle scattering and the transport of energy [e.g., *Fok et al., 1993; Liemohn et al., 2000; Khazanov et al., 2000*]. Density structures on a variety of scale sizes have been found in plasmaspheric plasma [*Sandel et al., 2003*]. An abrupt one to two orders of magnitude drop in plasma density often characterizes the outer boundary of the plasmasphere, referred to as the plasmapause, although this region may appear without a sharp gradient instead gradually falling in density to trough levels. The most significant azimuthal plasmaspheric structure is the plume, which extends sunward in afternoon and evening local times. The plume is created by the global cross-tail electric field induced by the solar wind streaming through the Earth's outer magnetic field [*Nishida, 1966; Grebowsky, 1970*].

Notches [*Sandel et al., 2003*] represent one of the largest density structures in the plasmasphere, along with the plasmasphere itself, the plasmaspheric plume, and plasmaspheric channels. They are characterized by deep density depletions that extend radially or mostly radially inward to  $L=2$  or less. The sizes in local time ranges from very narrow ( $\sim 0.1$  hours MLT) to very broad ( $\sim 3$  hours MLT). Notch densities observed by EUV are found to be a factor of 5-10 below the adjacent notch walls, although interior notch densities often fall to the EUV noise level so that notch depletions may be much deeper. Figure 1 shows three examples of plasmaspheric notches. Each panel is a 10-

minute integrated image acquired by the Extreme Ultraviolet (EUV) camera on the IMAGE mission. The camera observes 30.4 nm sunlight resonantly scattered by singly ionized helium ions in the plasmasphere. Counts increase logarithmically from dark blue to bright blue and then white. The Earth is in the center of each image and the bright arc close to the Earth is ionospheric glow on the sunward side. Panel (a) shows a structured notch toward the top of the image near dusk local time. Notches sometimes include a central prominence of enhanced plasma density that can be somewhat broad as in this case or exceptionally narrow and extending radially across two or more L-shells within the notch. Panel (b) shows one of the more narrow notches. The notch extends from about  $L=1.6$  to  $L=5.2$  before it can no longer be seen by the EUV instrument. Panel (c) shows a notch of similar simple structure, but much more broad in local time.

The present work explores the origin of these deep, large density cavities in the outer plasmasphere and their evolution. A distinct feature, such as a notch, presents the opportunity to follow its refilling and its motion across a wide range of L-shells. It is found that notches appear to share their origin with low-density channels, which are formed during recovery at the base of the plasmaspheric plume in the dusk region. In one notch, refilling is found to be consistent with previous early-time refilling, but also responsive to a brief increase in magnetic activity. Notches are also found to routinely drift eastward at a rate below corotation [*Sandel et al.*, 2003] and often at the same rate across a wide range of inner L-shells. As often seems to happen, the results of current work raises new questions that remain to be addressed in future efforts.

## Origin of a Notch

### *Observational Evidence*

Figure 2 shows the plasmasphere near the start of recovery from a period of enhanced convection. Each panel shows a plume in the dusk region that will soon drift eastward in the corotation direction. While otherwise similar, the first two events on May 31, 2000 and June 30, 2000 precede the formation of a notch. The third event on June 10, 2000 results in an extended low-density channel. These three event periods are shown again a short time later in Figure 3. A much more clear difference has developed in the plasma distribution between the first two (panels (a) and (b)) and the third event (panel (c)) as shown from left to right in the figure. The first two events develop into radial notch structures, while the third event forms a low density, azimuthal channel inside a wrapped plume. Of the few notches so far observed during formation, all appear to originate at the westward edge and base of the convection plume upon recovery from enhanced storm-time convection. The entrainment and wrapping of the convection plume during storm-time recovery was first proposed by *Grebowsky* [1970] and subsequently discussed in many studies [see for example, *Carpenter et al.*, 1992 and *Sandel et al.*, 2001]. The process results in an azimuthally extended and radially narrow region of low density inside a similarly extended region of enhanced density that was once the sunward extended plume.

Notches appear to originate in the same region during storm-time recovery.

Observationally, the distinction appears to be due to the size or plasma content of the storm-time plume and correspondingly the degree of plasmaspheric erosion. The top two events in Figure 2 are characterized by a thin plume and limited erosion of the plasmasphere. Much more of the outer plasmasphere was eroded in the bottom event in Figure 2. Careful examination of the events shown in Figures 1(a) and 3(b) reveal a thin wispy remnant of the convection plume over-draping the notch density cavity. While not always visible in EUV images, a remnant plume seems likely to remain after the formation of notches. The details of electric fields and other thermal plasma drivers that control the transition to a notch formation rather than a channel are left to subsequent analysis. It should be noted that in some cases extended low-density, channel-like structures are observed to reorient into radial low-density notches. Also, while the residual azimuthally draped plume in notch events quickly disappears from EUV images, an observationally similar, but slower thinning and drop in density is observed in the wrapped plumes that result in low-density channels [Grebowsky, 1970; Chen and Wolf, 1972; Adrian *et al.*, 2001].

In order to more easily examine notches, other plasmaspheric features, and variations in plasma content over time, subsequently shown EUV images are projected into the dipole magnetic equatorial plane and counts are transformed into pseudo-density, where modeled variations in solar irradiance at 30.4nm and the most dominant systematic influences of image intensity across the field of view are removed. The process used to perform this conversion is discussed in the Appendix.

A narrowing region of enhanced density that extends outward inside a large low-density notch also sometimes characterizes notch structure. An example of such a prominence is shown in Figure 1(a). In this example, the prominence is nearly as broad as the notch near the Earth and rapidly narrows in azimuth at larger distance such that it forms something like a “W” in enhanced density. Although not visible in this rendering of the event, prominences can sometimes be seen to extend across the entire radial length of the notch and with a very narrow azimuthal extent ( $\sim 0.1 R_E$ ).

This interior prominence can be seen forming just after notch formation during the event on June 24, 2000 shown in Figure 5. Pseudo-density images mapped into L-shell versus magnetic local time (MLT) are shown at about 30 minute intervals over a period of about 2 hours. Only that 5-hour MLT region centered on the notch is shown in each image. In the left most image the notch has freshly formed just westward of the recovering convection plume. The notch walls become more radial and distinct as the feature evolves, leaving an enhanced prominence near the notch center. While a definitive explanation for the formation of a notch prominence is not yet available, a candidate mechanism can be suggested.

### *Computational Explanation*

The candidate mechanism is best described by considering a few numerical experiment results. Figure 6 shows equatorial plane plots of plasmaspheric density from the dynamic

global core plasma model (DGCPM) [*Ober et al.*, 1997]. Results from two simulations are shown, one with a prescribed convection electric field description (Figure 6a) and one with an electric field that is self-consistently calculated from the inner magnetospheric field-aligned currents produced by a simulation of energetic ring current plasma (Figure 6b). Both plots are for the same instant during the recovery phase of the April 17, 2002 magnetic storm, and the details of the computational setup for these results are discussed by *Liemohn et al.* [2004].

Figure 6b exhibits several features that resemble the plasmaspheric notches seen in the IMAGE EUV data. At ~15 LT there is a small indentation in the plasmopause, near 18 LT is a V-shaped depletion corresponding to the wrap of the drainage plume around the storm-time plasmopause, and at ~21 LT is yet another depleted notch within the wrapped-up plume structure. These low-density regions are not seen in Figure 6a, and instead a smoothly-varying plasmopause with the traditional tear-drop-plus-drainage-plume morphology is evident. The initial conditions and the ionospheric source and loss terms for these two simulations are exactly the same; the only difference is the convection electric field specification. The field yielding the plasmasphere in Figure 6a is a well-behaved two-cell convection pattern, while the field used to produce the plasmasphere in Figure 6b is distorted from the standard two-cell scenario by a rather large potential well near midnight and several small-scale, transient electric potential vortices superposed on the main convection pattern.

The electric potential vortices appear because of injections of hot ions from the plasma sheet into the ring current region. These influxes of particles create localized pressure peaks, which must have field-aligned currents on the eastward and westward ends of the peak to close the asymmetric ring current loop. These field-aligned currents produce wells and peaks (eastward and westward ends, respectively) in the ionospheric electric potential pattern, which in turn can be mapped back out to the magnetosphere and alter the plasma flow through near-Earth space. The plasma motion is a clockwise flow around the electric potential peak (westward end) and a counterclockwise flow around the well (eastward end). The end result is a radial outward flow between the peak and the well and inward flow to the outside (in the azimuthal direction) of the well-peak pair. As the hot ion pressure peak drifts around the dusk side of the inner magnetosphere, the associated potential structure will also move westward through the region, eventually dissipating on the dayside.

The cold, plasmaspheric particles, which have essentially no magnetic drift, are therefore a tracer of the time-history of the convective drift pattern. The formation of a notch in the plasmopause greatly depends on the local time location and extent of the hot ion injection. During a storm, there are many successive injections from the plasma sheet into the inner magnetosphere, which could cause numerous indentations and undulations in the plasmopause. Of course, this ring-current-induced deformation of the plasmopause is highly dependent on the ionospheric conductance, which regulates the strength of the resulting ionospheric potential pattern through Ohm's law. This may contribute to why notches appear during certain geomagnetically disturbed times and not others.

## Notch Refilling

The conversion to pseudo-density, mapping into the magnetic equator, and tracking of features makes it relatively easy to follow changes in notch content as it evolves.

Notches are often found to persist as an identifiable structure for an extended period of time [*Sandel et al.*, 2003], which also enhances our ability to follow the refilling process.

Figure 7 shows a sequence of images that extend across the entire lifetime of a notch that formed on May 31, 2000. The first image was taken at 0859UT and is shown in the figure as 0000 hours. The following images to the right show the time in hours and minutes relative to this first image time. The notch remains a prominent feature for nearly 16 hours, after which it is seen to fill in. In order to estimate the filling rate, the pseudo-density in a region centered on the notch is averaged and then followed in time.

The regions for which pseudo-density is averaged are shown in the second panel of Figure 7 by the red boxes that extends in 0.5 intervals from L=2 to L=3.5 and for one hour on either side of the notch center.

The average density as a function of time for this notch is shown in Figure 8 and is found to vary considerably during the three IMAGE orbital passes when the notch can be followed. During the first 5-hours and from the innermost range to the outermost, refilling rates are  $5.5 \pm 21 \text{ cm}^{-3} \text{ d}^{-1}$ ,  $46.8 \pm 3.8 \text{ cm}^{-3} \text{ d}^{-1}$ , and  $49.4 \pm 9.9 \text{ cm}^{-3} \text{ d}^{-1}$ , respectively. As can be seen, the densities for the innermost L-shell range are essentially constant, while densities in the outer two L-shell ranges rise at similar rates. During the second

pass the notch is located between 7.1 hours and 8.6 hours MLT. Even in this post-dawn region plasma is lost throughout the notch during the modest increase in activity ( $K_p=3$ ) around 0000UT on June 1, 2000. From the innermost to the outermost L-shell ranges the loss rates are  $-101 \pm 45.5 \text{ cm}^{-3} \text{ d}^{-1}$ ,  $-128 \pm 29 \text{ cm}^{-3} \text{ d}^{-1}$ , and  $-129 \pm 30 \text{ cm}^{-3} \text{ d}^{-1}$ , respectively. Refilling is found again during 4-hours of observations on the last IMAGE pass. Refilling rates are  $75 \pm 18 \text{ cm}^{-3} \text{ d}^{-1}$ ,  $139 \pm 14 \text{ cm}^{-3} \text{ d}^{-1}$ , and  $80 \pm 11 \text{ cm}^{-3} \text{ d}^{-1}$ , from the innermost to outermost L-shell range. Unlike at the beginning of the observational period, there is clear refilling across the whole L-shell range during the third IMAGE apogee pass. As is expected, the average densities across all times are highest for L-shells in the range  $2.0 \leq L \leq 2.5$  and lowest in the range  $3.0 \leq L \leq 3.5$ . *Lawrence et al.* [1999] measured early time refilling at a rate of  $\sim 0.6\text{-}12 \text{ cm}^{-3} \text{ d}^{-1}$  and refilling at a later time of  $10\text{-}50 \text{ cm}^{-3} \text{ d}^{-1}$ . By using a dipole magnetic field, an estimate of about a factor of 50 difference in flux tube volume and hence refilling rate might be anticipated between the *Lawrence et al.* [1999] geosynchronous observations and those presented here. Based on that estimate, our early recovery-time refilling rates are comparable to those found at geosynchronous orbit.

### **Notch Drift**

In addition to following the refilling of plasmaspheric flux tubes, the cross-field drifts of 18 notches have been tracked. Notch centers near  $L=2.5$  are first approximated manually and then a Gaussian function is fit to the azimuthal profile in order to locate the notch center. Notch centers are then followed in time. Table 1 shows the azimuthal drift rates

as hours per day. A feature drifting with the Earth's rotation would be shown at a rate of 24 hours per day. Only one notch was observed to corotate with the Earth; the one observed on May 28, 2000. Most of the remaining notches drift at a rate between 85% and 97% of corotation. Two notches observed from December 21 to 23, were found to drift considerably slower at 44% and 74% the corotation rate. Figure 9 shows an example of a notch that could be followed for three days. The symbols show the MLT location of the notch center during the observational period. The solid line is a linear fit to the notch centers, which gives a drift rate that is 91% of the corotation rate. Were the notch to strictly corotate with the Earth, its location would follow the dotted line. While this notch was followed for a longer time than usual, the ability to approximate its subcorotation with a linear function is typical. Even when minor variations away from a linear fit are found, an overall linear drift with time dominates the behavior of a notch. In addition, notches often substantially maintain their spatial shape during their lifetime. Some of the apparent changes in notch structure may be attributed to changes in observing geometry, which is why closer examination of the evolution of notch shape is left for subsequent study.

*Burch et al.* [2004] have proposed that subcorotation of the plasmasphere is driven by subcorotation of the ionosphere. They go on to propose that the ionospheric disturbance dynamo drives ionospheric motion relative to corotation as described by *Blanc and Richmond* [1980]. The assertion was demonstrated by comparing ionospheric drift measurements from the DMSP spacecrafts against EUV derived plasmaspheric drift. The present notch measurements offer another opportunity to test this hypothesis. Ion Drift

Meter (IDM) observations from the DMSP spacecraft numbers F12, F13, and F15 have been used to obtain average drift for time periods when a DMSP orbit passes within the L-shell range  $2 \leq L \leq 3$  and within 2 hours MLT of the notch location as observed by IMAGE. IDM drift measurements during these conjunctions are averaged and included in Table 1. The relative correspondence between derived notch drift rates and ionospheric drift rates can be seen in Figure 10. Within the margin of error, most average ionospheric drifts are consistent with notch drift.

Notably, that is not true for all cases. One of those cases is highlighted in Figure 11. Here the individual IDM drift measurements can be compared to the derived linear notch drift along side the individual notch locations relative to the linear drift. IDM drift measurements are shown in the upper panel. Each symbol is an ionospheric drift measurement. Each grouping of symbols results from one DMSP pass near the notch location. The dotted line corresponds to corotation. The solid red line is the linear drift of the notch. Ionospheric drift rates are systematically slower than that of the notch. In the lower panel the relative magnetic longitude of the notch, in hours, is plotted through the observational period. The solid line is the linear fit. The dotted line is again for strict corotation. As mentioned above, it is not uncommon to find the observed notch location to drift somewhat slower and faster than the long-term trend, but identification of a long-term trend appears well justified.

Green and red colors are used in Figure 11 to represent notch location in and out of sunlight, respectively. This annotation was applied to the analysis of all events for the

purpose of revealing whether the day/night changes in ionospheric conductivity might contribute to a diurnally varying slippage of the notch location relative to the long-term drift. No such dependence was found. Observational geometry was also considered as a possible source of apparent short-term shifts in notch position. In a format similar to Figure 11, the spacecraft angular location relative to the plane of the notch and the rate of spacecraft motion transverse to the plane of the notch were examined along side the short-term shifts in notch position relative to the long-term trend. The idea here is that an observing location out of the plane of a notch might result in a systematic error in locating the notch in magnetic longitude. Similarly, the rate of motion of the observing location toward or away from the notch might lead to a systematic increase or decrease of the apparent rate of motion of a notch. Again, no systematic correlation could be found to explain these short-term shifts.

Another explanation for the notch (and, in general, plasmaspheric) subcorotation is the dawn-dusk asymmetry of the electric potential pattern [e.g., *Lu et al.*, 1989; *Boonsiriseth et al.*, 2001; *Ridley et al.*, 2004]. For instance, *Lu et al.* [1989] found that the potential difference from the pole to the equator along the dusk meridian is typically 1.5 times larger than the potential difference along the dawn meridian. *Ridley et al.* [2004] goes on to explain this asymmetry as a result of the Hall conductance gradient at the terminators. The net effect is to reduce the magnitude of the dawnside potential peak and increase the size of the duskside potential well (compare Plates 4 and 6 of *Ridley et al.* [2004]). The potential pattern asymmetry results in a stronger sunward convection on the duskside of the magnetosphere than on the dawnside, which is a difference not accounted for in

standard two-cell convection patterns. The symmetric convection scenario leads to subcorotative flow (or even stagnation) on the duskside and supercorotative flow on the dawnside, and the net influence of convection is zero on the drift period along closed drift paths (in steady state). However, the convective asymmetry creates a larger decrease on the duskside and a smaller increase on the dawnside, resulting in subcorotative drift periods. *Liemohn et al.* [2004] show that the inner magnetospheric component of the dawn-dusk asymmetry varies with storm phase (in the self-consistent electric field results), indicating that the subcorotation effect is modulated by field-aligned current and conductance variations. The disturbance dynamo discussed by *Burch et al.* [2004] also causes subcorotative drift periods. Both effects will cause the same net westward flow in the DMSP drift data. The relative contribution of these two effects is beyond the scope of this paper and reserved for a later study.

## **Discussion and Conclusions**

Notches are one of the remarkable large-scale structural features of the plasmasphere, only recognized after flight of the remote sensing EUV instrument on the IMAGE spacecraft. Notches are characterized by nearly radial cavities in plasma density that often extend over  $2 R_E$  in the magnetic equator and from a tenth of an hour to two hours or more in magnetic local time. The notch density cavity can extend inward to  $L=1.6$  or less and is sometimes found to be transiently “capped” at the outer plasmaspheric boundary by a thin, residual plasmaspheric plume. Densities in a notch can be at least a factor of 5-10 lower than the adjacent notch walls. Notches appear to form following

weak periods of enhanced convection on the westward edge and base of the plasmaspheric plume. They can maintain their form for several days during quite conditions as well as loose plasma while maintaining shape during subsequent weak periods of increased magnetic activity.

A central enhanced density prominence was found in about 22% of the notches identified in 2000. On June 24, 2000, a prominence was observed to form soon after or with formation of a notch. Evidence is presented here that this prominence may be indicative of a spatially localized injection of plasma sheet ions and the formation of enhanced meso-scale regions of opposite electric potential. These small-scale potential enhancements appear capable of locally drawing plasma out of the interior high-density region into the low-density notch through localized modification of the  $\mathbf{E} \times \mathbf{B}$  convection pattern. Although not presented, notch prominences do not necessarily stay centered in the notch even though the notch itself maintains its general shape. In two cases interior prominences are observed to drift westward relative to the notch, later merging with the notch interior wall.

The large low-density region of a notch lends itself to the study of plasmaspheric refilling and examination of cross-field drift over extended periods of time. Average pseudo-densities in the magnetic equatorial plane are shown here in Figure 7 for May 31 and June 1, 2000. During the first observational pass the plasmasphere is in a period of recovery from a moderate storm ( $Kp_{\max}=4+$ ). Changes in average density in the innermost L-shell range is somewhat mixed with little overall refilling. The middle and

outer L-shell range, however, show a similar rate of refilling in the range of  $47\text{-}49\text{ cm}^{-3}\text{d}^{-1}$ . Refilling between 2 and 3 times this rate is observed during the third IMAGE orbital pass in all L-shell ranges. This last period of early-time refilling is observed when the densities are higher than that present for the first orbital pass observing period. These refilling ranges are consistent with those reported by *Lawrence et al.* [1999], given an estimate of the approximate difference in flux tube volume between geosynchronous orbit and those presented here.

Of some interest is the loss of plasma in the innermost L-shell range ( $2.0 \leq L \leq 2.5$ ) during the modest increase in magnetic activity to  $K_p=3$  near the start of June 1, 2000. Based on *Carpenter and Anderson* [1992], the plasmopause might be expected to erode inward to  $L=3$  for this level of activity. However, essentially the same rate of plasma loss is seen inside that L-shell as is seen outside. Convective plasma loss cannot explain what is found inside of  $L=3$ . *Carpenter* [1962] is the first to report this type of plasma loss inside a storm-time plasmopause. Drainage into the ionosphere appears to be the only other avenue for plasma loss, which was first proposed by *Park* [1973]. Successful explanation of this low L-shell plasmaspheric erosion will also need to operate near dawn as found here.

As a plasmaspheric feature extended in L-shell, notches directly support the examination of convective drift across a significant range of L-shells. Table 1 summarizes our findings for 18 notches observed during 2000. Only one of these notches was found to drift with the rotation of the Earth. The only conclusion we can reach is that the

plasmasphere usually lags corotational motion. However the slippage is often not large. We find the plasmasphere most often drifts eastward at a rate of 85%-97% of corotation. In two cases, the plasmasphere drifted much slower, as slow as 44% of corotation. *Burch et al.* [2004] has suggested that westward ionospheric drift is responsible for slowing the corotational motion of the plasmasphere. Just as in this cited study, we have obtained ionospheric drift measurements from the DMSP IDM experiment. Ionospheric drifts were obtained for 12 of 18 notches and one standard deviation error estimates for these drifts suggests most are consistent with our notch drift rates.

For two of the notches studies here, the IDM drift rates are significantly slower than found using EUV. The case in August 2000 has been examined more closely using Figures 9, 10, and 11. A possible explanation for the differences found between IDM and EUV drifts might be due to magnetic local time differences in the observations. As stated above, the IDM measurements included in ionospheric drift averages are within two hours MLT of the IMAGE spacecraft location. Should there exist variation in ionospheric drift on smaller azimuthal scales, then the different drifts found here do not contradict the ionospheric slippage proposed by *Burch et al.* [2004]. In an attempt to test that possibility, IDM measurements have been resampled for the August 2000 notch with a much more strict MLT criteria for correspondence. In this case, DMSP was required to be within 0.5 hours MLT of the EUV-observed notch at the time of the observation in addition to being between L=2 and L=3. Three of the nine DMSP orbital passes shown in Figure 11 are within 0.5 hours MLT of the notch center. The drifts measured by IDM are still easily lower in drift rate than that obtained from the EUV instrument. The IDM

measurements were obtained from the University of Texas at Dallas and include quality flags that are intended to reflect the likelihood that IDM measurements accurately reflect ionospheric drifts. Only those measurements assigned the highest quality flag were included in this study. While the other DMSP average drifts are statistically consistent with the notch drifts derived here, there remains considerable scatter in DMSP drift values. The implication is that the explanation for subcorotational drift of the plasmasphere may be more complex than currently thought. In this regard, we note the works of *Lu et al.* [1989], *Boonsiriseth et al.*, 2001, *Ridley et al.* [2004], and *Liemohn et al.* [2004] may provide an additional explanation for subcorotational drift. These works collectively suggest that Hall conductance gradients at the terminators cause a dawn-dusk electric potential asymmetry, yielding a net subcorotational plasmaspheric drift that is storm-phase dependent.

## Appendix

Counts are converted to column density [Sandel, private communication] using the following expression:

$$N = a \cdot 1.89 \times 10^{19} / F ,$$

where  $N$  is the He<sup>+</sup> column abundance in cm<sup>-2</sup>,  $a$  is the EUV signal in counts/pixel for a 10 minute integration, and  $F$  is the solar irradiance at 30.4 nm in units of

$photons \cdot cm^{-2} \cdot s^{-1}$ . Solar irradiance is obtained from the SOLAR2000 irradiance model [Tobiska 2003].

Column integrated density is converted to pseudo-density by dividing by an estimate of the distance along the line of sight that contributes most to the image intensity at each location in the field of view. Due to rapidly falling densities in the plasmasphere with increasing L-shell, the innermost regions penetrated by a given line of sight will contribute most to the observed 30.4nm intensity [Sandel *et al.*, 2003]. The EUV imager spatial resolution in the equatorial plane while observing from apogee is about 0.1  $R_E$ , therefore that distance along the line of sight when passing within 0.1  $R_E$  of the innermost L-shell reached is divided into the column integrated density for each position in the EUV field of view. A sketch describing this influence is shown in Figure 4 along with a typical example of how this effective integration length changes with line of sight below a high latitude observing location.

By choosing observing periods when the IMAGE spacecraft is at high latitude (>60 degrees magnetic latitude) and relatively far from perigee (>4  $R_E$  geocentric distance), the regions dominating the intensities observed in EUV images are relatively close the magnetic equator. Relatively little change in density within the plasmasphere is anticipated along magnetic field lines near the equator [Gallagher, *et al.*, 2000 and Reinisch *et al.*, 2003], therefore EUV images are next mapped to the dipole magnetic equator [Goldstein *et al.*, 2003]. Dipole coordinates are used, since distortions from

dipole are small close to the Earth during the periods of quiet geomagnetic activity examined in this study.

The quantitative accuracy of the pseudo-density calculation has been tested by comparison to a known density. The dynamic global core plasma model (DGCPM) [Ober *et al.*, 1997] was used to simulate a storm-time recovery period on June 10, 2001. The simulation resulted in a nightside, narrow plume and otherwise normal plasmasphere with a relatively sharp plasmopause boundary. This equatorial distribution of plasma was then used to define densities along the magnetic field. This run of DGCPM does not include an ionosphere and is limited to modeling L-shells beyond 2, therefore no model ionosphere is included in this test. Simulated EUV images through this modeled environment were then produced for satellite positions at a distance of  $8 R_E$  and at magnetic latitudes of  $60^\circ$ ,  $70^\circ$ ,  $80^\circ$ , and  $90^\circ$ . Pseudo-densities were then computed for each image and compared to the original density distribution. Accuracy improved notably with increasing latitude, especially in the region viewed on the far side of the Earth. Most derived densities are within about 50% of the original, but vary by as much as a factor of nearly 10 in localized regions. Density at a sharp plasmopause tended to be underestimated. Densities just inside the plasmaspheric plume, in the low-density channel over draped by the plume, are over estimated. Naturally densities in the Earth's shadow are underestimated by the pseudo-density calculation.

## **Acknowledgements**

The IMAGE Mission through the NASA Office of Space Science has supported this research. The DMSP drift meter data were provided by the Center for Space Sciences at the University of Texas at Dallas through their website at <http://cindispace.utdallas.edu/DMSP/>.

## References

- Adrian, M.L., D.L. Gallagher, J.L. Green, and B.R. Sandel, The large-scale plasmaspheric density trough associated with the 24 May 2000 geomagnetic storm: IMAGE EUV observations and Global Core Plasma Modeling, *Eos*, *82*, S352, 2001.
- Blanc, M., and A. D. Richmond, The ionospheric disturbance dynamo, *J. Geophys. Res.*, *85*, 1669-1686, 1980.
- Boonsiriseth, A., R. M. Thorne, G. Lu, V. K. Jordanova, M. F. Thomsen, D. M. Ober, and A. J. Ridley, A semiempirical equatorial mapping of AMIE convection electric potentials (MACEP) for the January 10, 1997, magnetic storm, *J. Geophys. Res.*, *106*, 12, 903, 2001.
- Burch J. L., J. Goldstein, B. R. Sandel (2004), Cause of plasmasphere corotation lag, *Geophys. Res. Lett.*, *31*, L05802, doi:10.1029/2003GL019164.
- Carpenter, D. L., The magnetosphere during magnetic storms, a whistler analysis, Ph.D. thesis, *Tech. Rep. 12*, Radiosci. Lab., Stanford Univ., Stanford, Calif., June 1962.

- Carpenter, D. L., A. J. Smith, B. L. Giles, C. R. Chappell, and P. M. E. Decreau, A case study of plasma in the dusk sector associated with enhanced magnetospheric convection, *J. Geophys. Res.*, *97*, 1157, 1992.
- Chen, A. J. and R. A. Wolf, Effects on the plasmasphere of a time-varying convection electric field, *Planet. Space Sci.*, *20*, 483, 1972.
- Fok, M-C., J. U. Kozyra, A. F. Nagy, C. E. Rasmussen, and G. V. Khazanov, A decay model of equatorial ring current and the associated aeronomical consequences, *J. Geophys. Res.*, *98*, 19,381, 1993.
- Goldstein, J., B. R. Sandel, M.R. Hairston, and P. H. Reiff, Control of plasmaspheric dynamics by both convection and sub-auroral polarization stream, *Geophys. Res. Lett.*, *30(24)*, 2243, doi:10.1029/2003GL018390, 2003.
- Grebowsky, J. M, Model study of plasmaspheric motion, *J. Geophys., Res.*, *75*, 4329, 1970.
- Khazanov, G.V., K. V. Gamayunov, V. K. Jordanova, Self-consistent model of magnetospheric ring current and electromagnetic ion cyclotron waves: The May~2-7, 1998, storm, *J. Geophys. Res.*, *108(A12)*, 1419, doi: 10.1029/2003JA009833, 2003b.
- Lemaire, J. F., and K. I. Gringauz, *The Earth's Plasmasphere*, Cambridge University Press, New York, 1998.
- Lawrence, D. J., M. F. Thomsen, J. E. Borovsky, and D. J. McComas, Measurements of early and late time plasmasphere refilling as observed from geosynchronous orbit, *J. Geophys. Res.*, *104*, 14,691-14,704, 1999.

- Liemohn, M. W., J. U. Kozyra, P. G. Richards, G. V. Khazanov, M. J. Buonsanto, and V. K. Jordanova, Ring current heating of the thermal electrons at solar maximum, *J. Geophys. Res.*, *105*, 27,767, 2000.
- Liemohn, M. W., A. J. Ridley, D. L. Gallagher, D. M. Ober, and J. U. Kozyra, Dependence of plasmaspheric morphology on the electric field description during the recovery phase of the April 17, 2002 magnetic storm, *J. Geophys. Res.*, *109*(A3), A03209, doi: 10.1029/2003JA010304, 2004.
- Lu, G., P. H. Reiff, M. R. Hairston, R. A. Heelis, and J. L. Karty, Distribution of convection potential around the polar cap boundary as a function of the interplanetary magnetic field, *J. Geophys. Res.*, *94*, 13,447, 1989.
- Nishida, A., Formation of the plasmopause, or magnetospheric plasma knee, by the combined action of magnetosphere convection and plasma escape from the tail, *J. Geophys. Res.*, *71*, 5669, 1966.
- Ober, D. M., J. L. Horwitz, and D. L. Gallagher, Formation of density troughs embedded in the outer plasmasphere by subauroral ion drift events, *J. Geophys. Res.* *102*, 14,595, 1997.
- Park, C. G., Whistler observations of the depletion of the plasmasphere during a magnetospheric substorm, *J. Geophys. Res.*, *78*, 672-683, 1973.
- Reinisch, B. W., X. Huang, P. Song, J. L. Green, S. F. Fung, V. M. Vasyliunas, D. L. Gallagher, and B. R. Sandel, Plasmaspheric Mass Loss and Refilling as a Result of a Magnetic Storm, *J. Geophys. Res.*, 2003JA009948RR.
- Ridley, A. J., T. I. Gombosi, and D. L. De Zeeuw, Ionospheric control of the magnetosphere: Conductance, *Ann. Geophys.*, *22*, 567, 2004.

Sandel, B. R., R. A. Kind, W. T. Forrester, D. L. Gallagher, A. L. Broadfoot, and C. C.

Curtis, Initial results from the IMAGE extreme ultraviolet imager, *Geophys. Res., Lett.* 28, 1439-1442, 2001.

Sandel, B. R., J. Goldstein, D. L. Gallagher, M. Spasojevic, Extreme ultraviolet imager observations of the structure and dynamics of the plasmasphere, *Space Science Reviews*, 109, 25-46, 2003.

Tobiska, W.K., SOLAR2000 irradiances for climate change, aeronomy, and space system engineering, *Adv. Space Res.*, submitted, 2003.

## Figure Captions:

Figure 1: Examples of plasmaspheric notches are shown in EUV observations from 2000. Each panel is shown with the day of year and universal time of the observation. They are found to extend over 2 or more L-shells, be as narrow as 0.1 MLT and as broad as several hours MLT. Notches can be simple gaps in density or contain structure such as the interior prominence shown in the top-middle image.

Figure 2: Storm-time recovery of the plasmaspheric plume on three different days is shown. Two of the days on May 31, 2000 and June 30, 2000 result in the formation of a notch. June 10, 2000 results in the formation of a low density channel.

Figure 3: EUV images of the plasmasphere show notches and a channel formed later in storm-time recovery on the days shown in Figure 2. Panels (a) and (b) are notches early in the formation process. Panel (c) shows a channel still forming.

Figure 4: The lowest L-shells contribute most to observed 30.4nm light intensity due to strongly falling densities in the plasmasphere. The line of sight distance through the lowest L-shells effectively increases as a high latitude imager looks further from the Earth. The sketch in the lower left outlines the effect. The plot in the upper right displays a typical change in effective integration length with imaged L-shell. Up to a factor of about three change in the contribution of a given density to observed 30.4nm intensity can result in an imager's field of view.

Figure 5: A prominence is shown forming inside the notch that developed on June 24, 2000. Universal time is shown toward the bottom in each panel, where EUV intensities have been projected into the dipole magnetic equatorial plane and expressed in pseudo-density.

Figure 6: Equatorial plane plasmaspheric density plots from the DGCPM for the recovery phase of the April 17, 2002 magnetic storm. The two results use (a) a smoothly-varying two-cell convection pattern and (b) a convection pattern generated self-consistently from a concurrent ring current simulation. The view is from over the north pole with noon to the left and distances are given in  $R_E$ .

Figure 7: The notch formed on May 31, 2000 is sampled in these images throughout its life. Times shown are relative to the time of the first image of 0831UT on this day. It can be seen that the notch extends across roughly  $2 R_E$  in radial distance and 2 hours MLT in EUV images. Plasmaspheric content is integrated across the region shown by the box outline on the image at 0140 hours.

Figure 8: Integrated density from  $L=2$  to  $L=3.5$  and for 2 hours local time centered on the notch in the event series shown in Figure 7 are normalized by the integration area to give average density as a function of time through the event. Marked by the horizontal line, the density remains roughly constant at an average of  $57 \pm 4 \text{ cm}^{-3}$  for the first 16 hours.

The average density increases at a rate of  $98 \pm 11 \text{ cm}^{-3}/\text{day}$  during the last 4 hours before the notch feature disappears in EUV images.

Figure 9: A notch center is tracked across three days in August 2000 and shown as "+" symbols. The solid line is a linear fit to the azimuthal notch drift at  $21.9 \pm 0.07$  hours/day. The dotted line indicates corotational drift.

Figure 10: A scatter plot is shown for EUV derived plasmaspheric and IDM derived ionospheric drifts. Error bars are drawn one standard deviation to either side of the average drifts.

Figure 11: Drift rate derived from the IDM on DMSP satellites is shown in the upper panel as a function of time on June 24-25, 2000. Each collection of symbols represents a separate DMSP pass through the vicinity of the notch in space and time. The dotted line corresponds to strict corotation. The red line is the notch drift derived from the EUV instrument. The bottom panel shows the magnetic drift of the notch relative to the initial time of the observation period. The solid line is a least squares fit to the notch location. The dotted line represents strict corotation. Green symbols are for dayside notch locations, while red symbols are for the nightside.

**Table 1: Plasmaspheric notch and ionospheric drifts**

<b>Dates in 2000</b>	<b>IMAGE/EUV (hrs/day)</b>	<b>DMSP/IDM (hrs/day)</b>
May 27	22.2 ± 0.12	21.2 ± 1.5
May 28	24.0 ± 0.09	-
May 31-June 1	22.4 ± 0.08	22.5 ± 3.4
June 14-15	20.4 ± 0.07	24.3 ± 3.7
June 16-17	22.6 ± 0.08	24.7 ± 1.4
June 24-25	23.2 ± 0.06	21.0 ± 0.5
June 30	21.6 ± 0.07	20.5 ± 20.5
July 1	22.5 ± 0.13	24.1 ± 1.8
July 3-5	22.6 ± 0.11	16.6 ± 1.0
July 6-9	22.2 ± 0.06	-
July 12-14	21.9 ± 0.64	22.6 ± 1.1
July 27-28	20.7 ± 0.11	22.0 ± 1.3
July 30-31	22.8 ± 0.05	21.0 ± 21.0
August 6	19.5 ± 0.76	-
August 6-10	21.9 ± 0.07	-
December 21-22	10.5 ± 0.08	-
December 22-23	17.8 ± 0.16	-
December 28-31	22.1 ± 0.10	21.8 ± 1.1

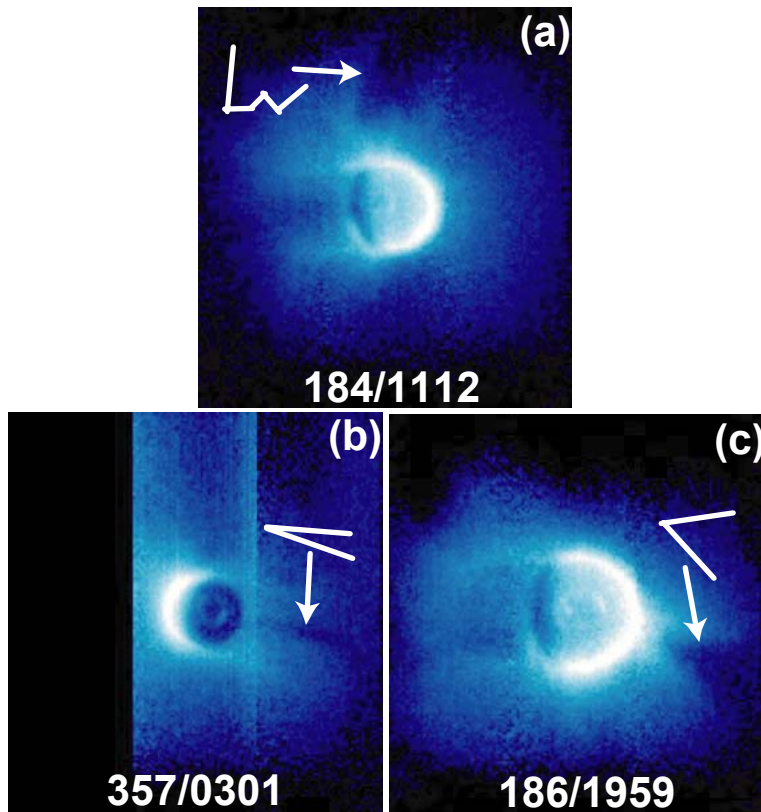
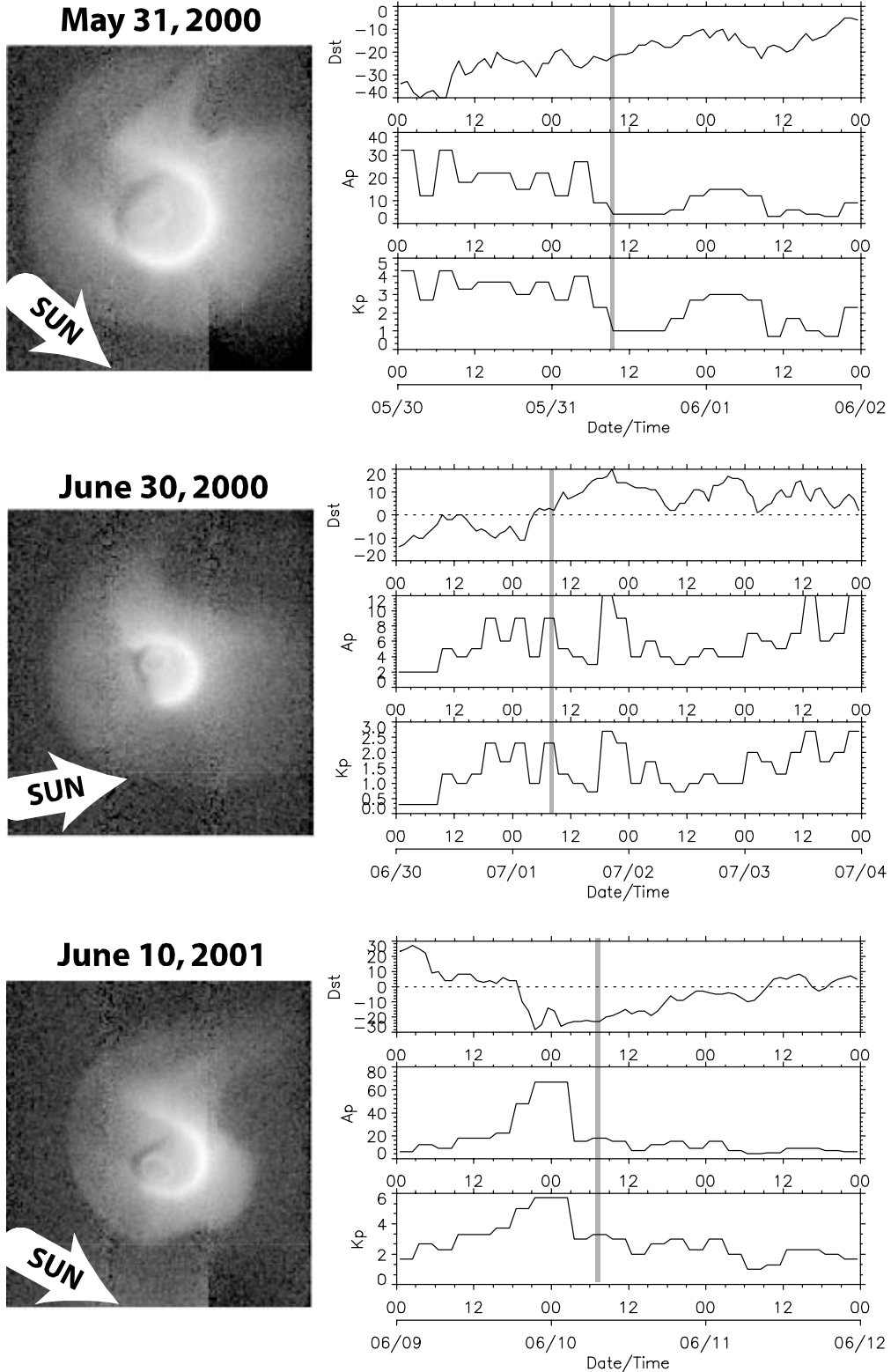


Figure 1: Examples of plasmaspheric notches are shown in EUV observations from 2000. Each panel is shown with the day of year and universal time of the observation. They are found to extend over 2 or more L-shells, be as narrow as 0.1 MLT and as broad as several hours MLT. Notches can be simple gaps in density or contain structure such as the interior prominence shown in the top-middle image.



**Figure 2: Storm-time recovery of the plasmaspheric plume on three different days is shown. Two of the days on May 31, 2000 and June 30, 2000 result in the formation of a notch. June 10, 2000 results in the formation of a low density channel.**

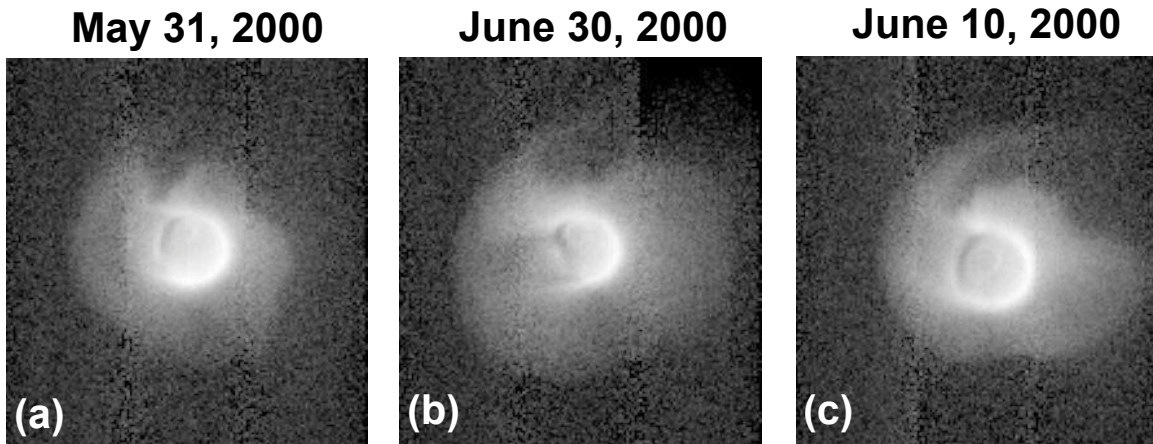


Figure 3: EUV images of the plasmasphere show notches and a channel formed later in storm-time recovery on the days shown in Figure 2. Panels (a) and (b) are notches early in the formation process. Panel (c) shows a channel still forming.

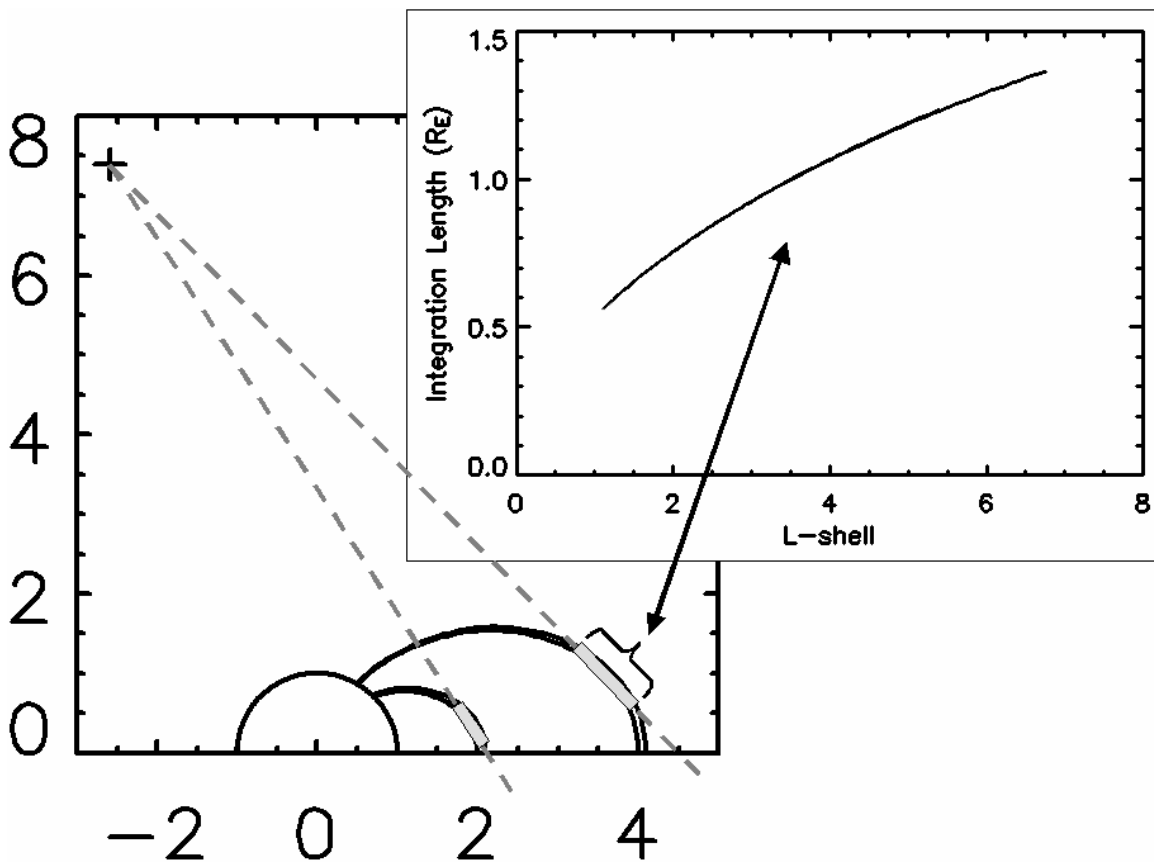


Figure 4: The lowest L-shells contribute most to observed 30.4nm light intensity due to strongly falling densities in the plasmasphere. The line of sight distance through the lowest L-shells effectively increases as a high latitude imager looks further from the Earth. The sketch in the lower left outlines the effect. The plot in the upper right displays a typical change in effective integration length with imaged L-shell. Up to a factor of about three change in the contribution of a given density to observed 30.4nm intensity can result in an imager's field of view.

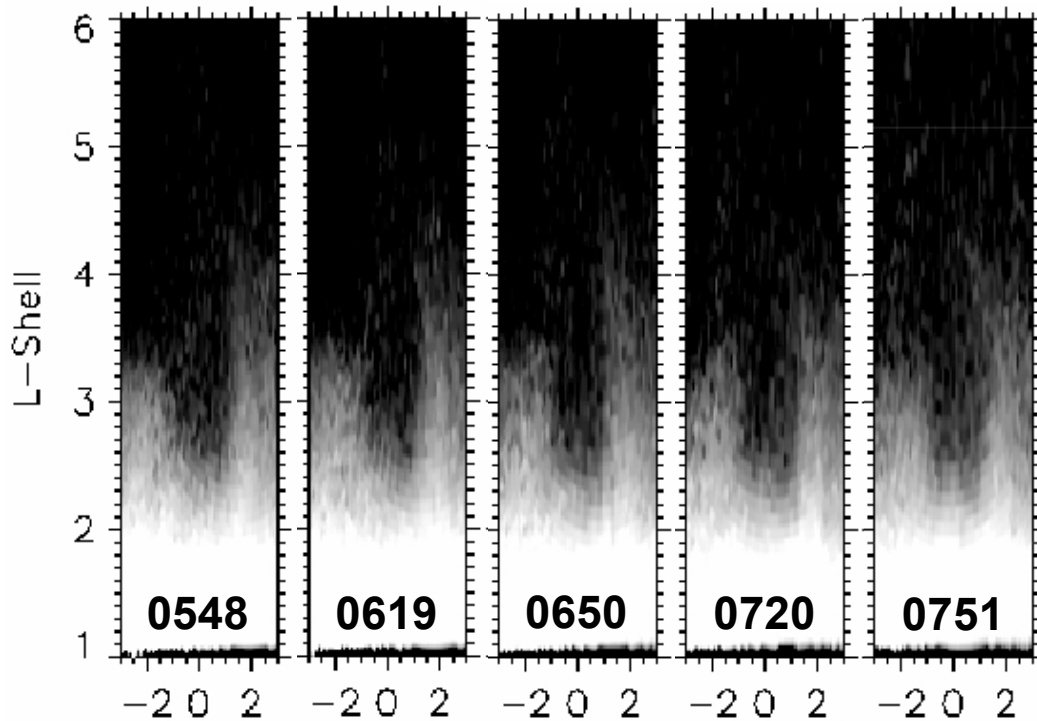


Figure 5: A prominence is shown forming inside the notch that developed on June 24, 2000. Universal time is shown toward the bottom in each panel, where EUV intensities have been projected into the dipole magnetic equatorial plane and expressed in pseudo-density.

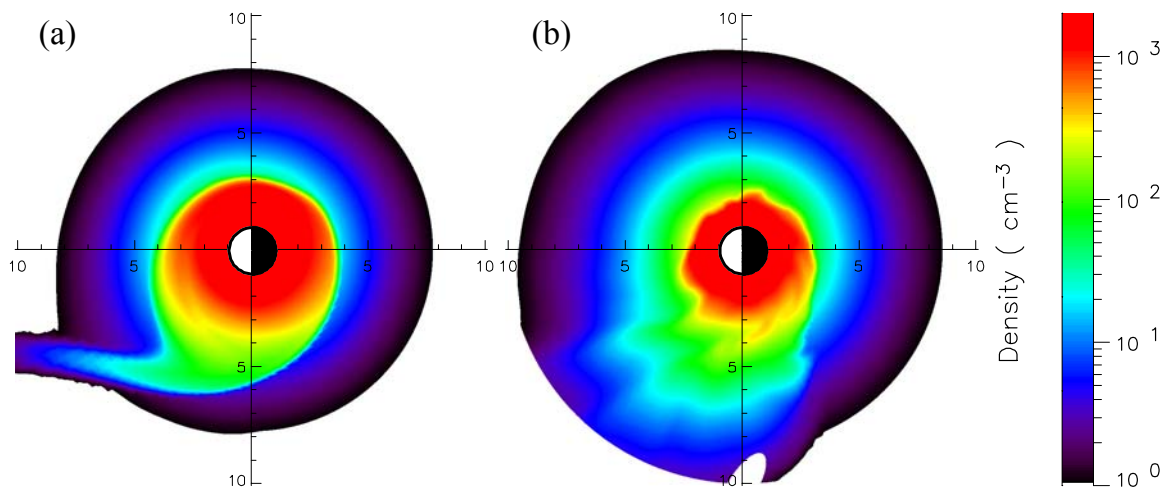
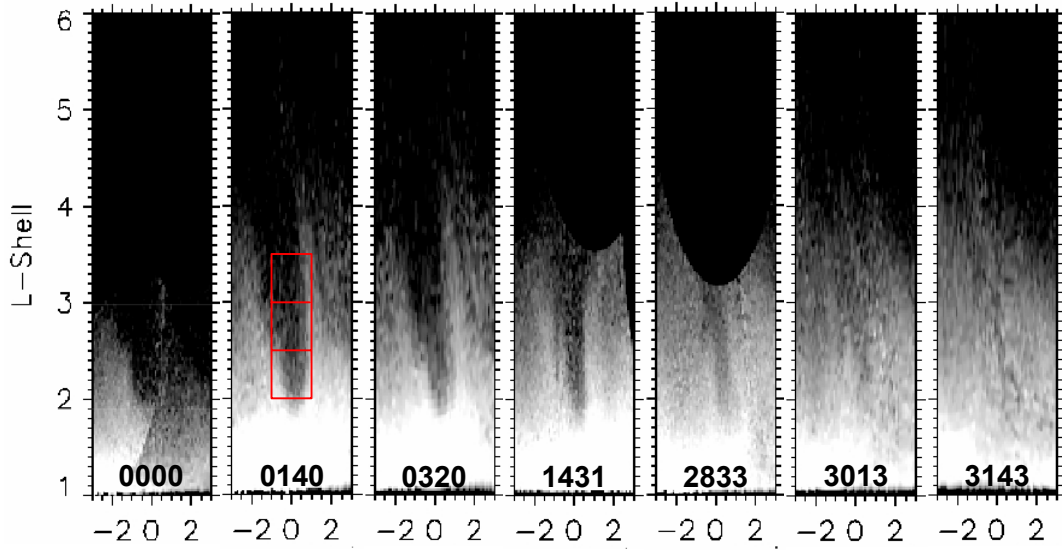


Figure 6: Equatorial plane plasmaspheric density plots from the DGCPM for the recovery phase of the April 17, 2002 magnetic storm. The two results use (a) a smoothly-varying two-cell convection pattern and (b) a convection pattern generated self-consistently from a concurrent ring current simulation. The view is from over the north pole with noon to the left and distances are given in  $R_E$ .



**Figure 7: The notch formed on May 31, 2000 is sampled in these images throughout its life. Times shown are relative to the time of the first image of 0831UT on this day. It can be seen that the notch extends across roughly  $2 R_E$  in radial distance and 2 hours MLT in EUV images. Plasmaspheric content is integrated across the region shown by the box outline on the image at 0140 hours.**

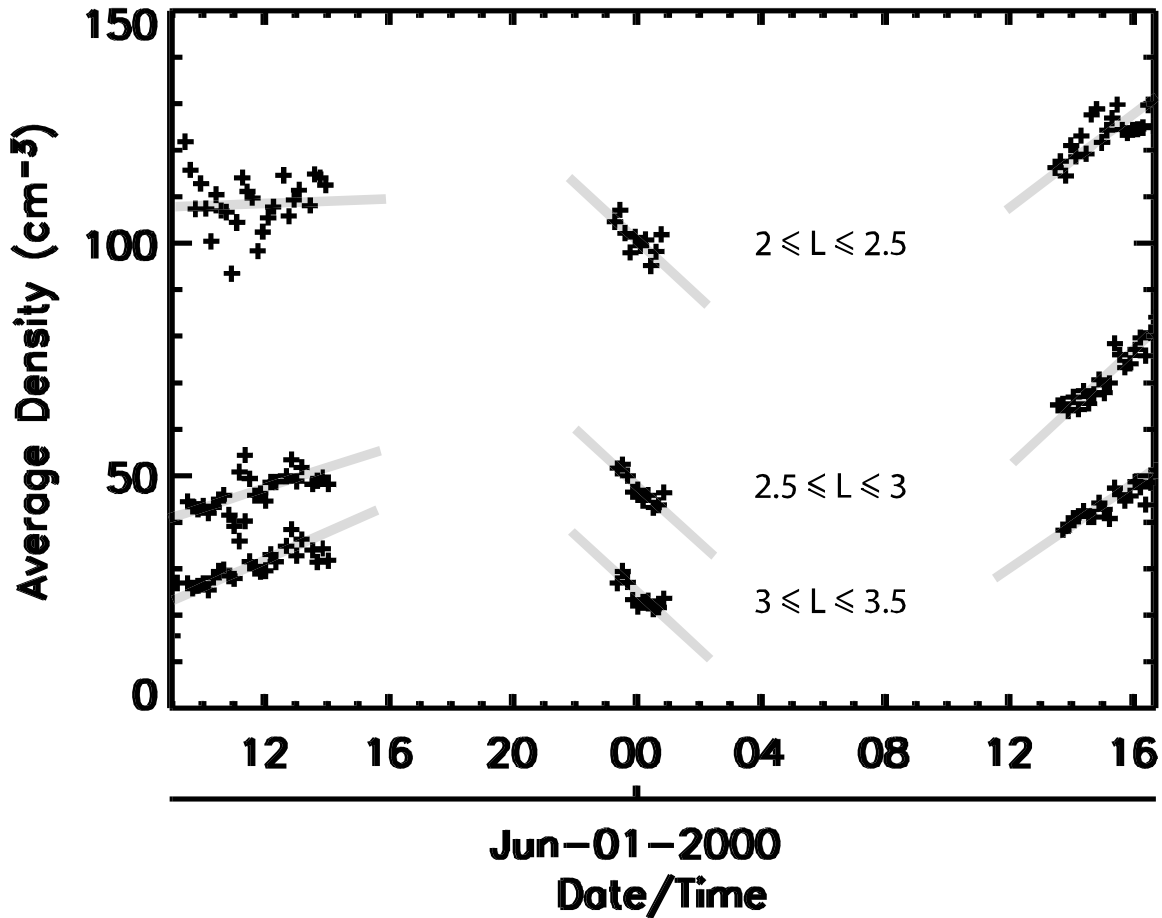


Figure 8: Integrated density from  $L=2$  to  $L=3.5$  and for 2 hours local time centered on the notch in the event series shown in Figure 7 are normalized by the integration area to give average density as a function of time through the event. Marked by the horizontal line, the density remains roughly constant at an average of  $57 \pm 4 \text{ cm}^{-3}$  for the first 16 hours. The average density increases at a rate of  $98 \pm 11 \text{ cm}^{-3}/\text{day}$  during the last 4 hours before the notch feature disappears in EUV images.

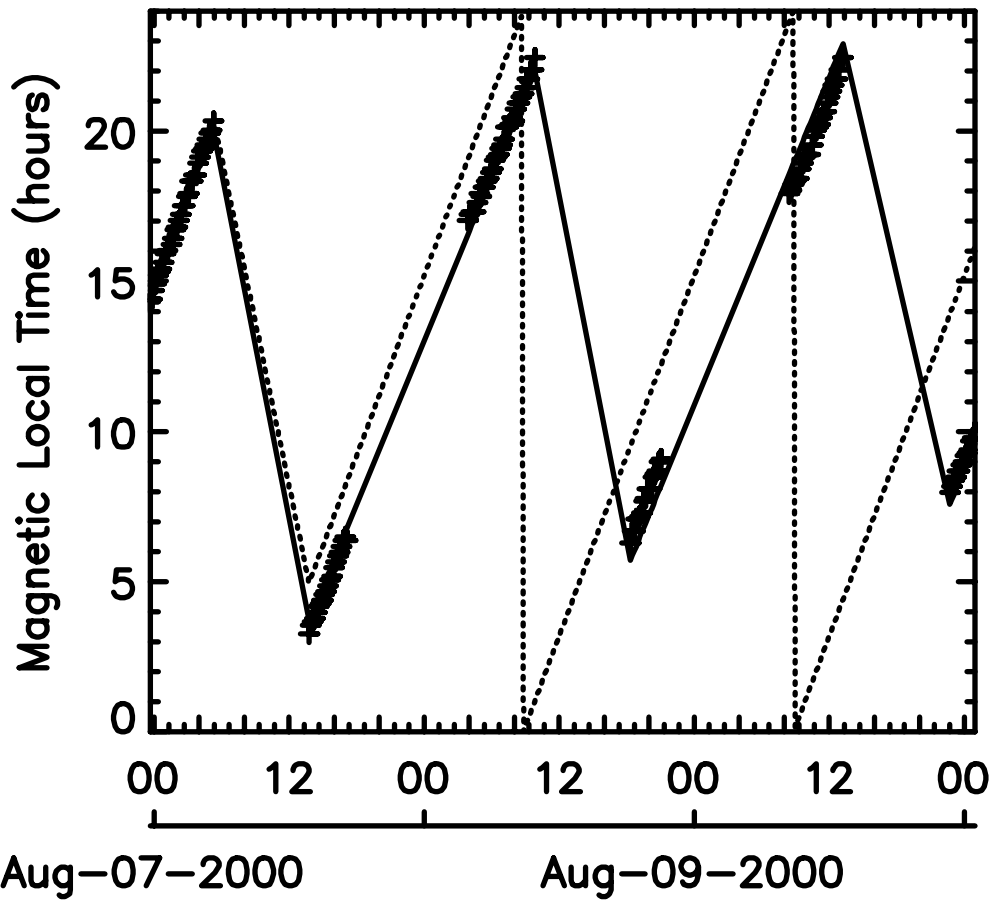


Figure 9: A notch center is tracked across three days in August 2000 and shown as "+" symbols. The solid line is a linear fit to the azimuthal notch drift at  $21.9 \pm 0.07$  hours/day. The dotted line indicates corotational drift.

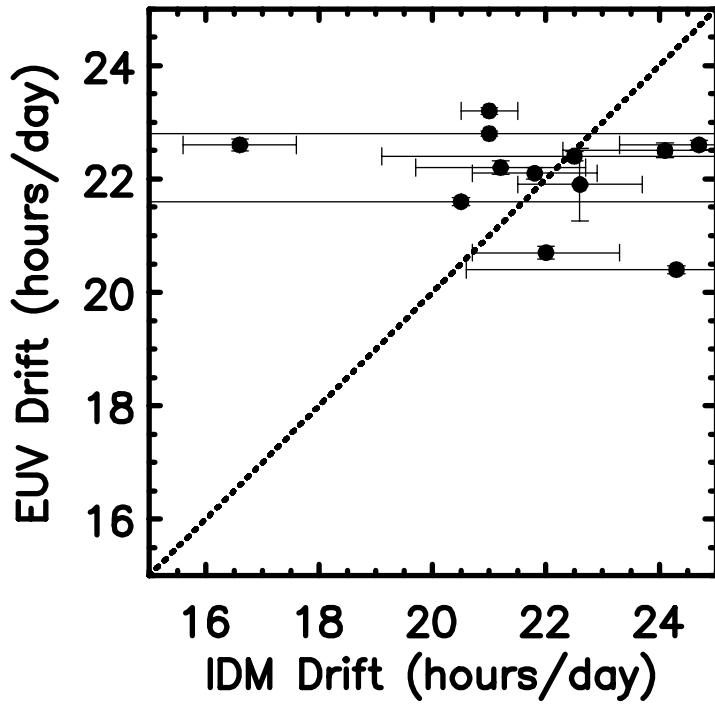


Figure 10: A scatter plot is shown for EUV derived plasmaspheric and IDM derived ionospheric drifts. Error bars are drawn one standard deviation to either side of the average drifts.

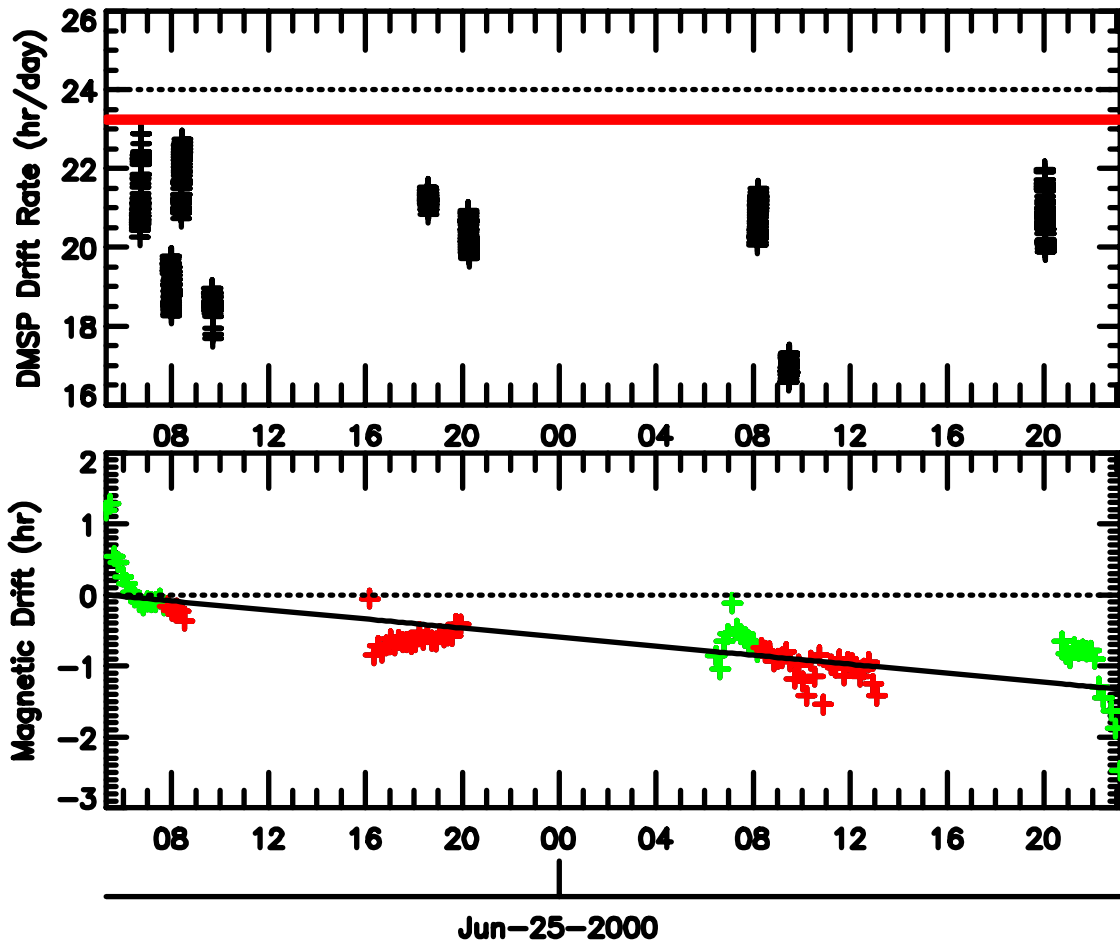


Figure 11: Drift rate derived from the IDM on DMSP satellites is shown in the upper panel as a function of time on June 24-25, 2000. Each collection of symbols represents a separate DMSP pass through the vicinity of the notch in space and time. The dotted line corresponds to strict corotation. The red line is the notch drift derived from the EUV instrument. The bottom panel shows the magnetic drift of the notch relative to the initial time of the observation period. The solid line is a least squares fit to the notch location. The dotted line represents strict corotation. Green symbols are for dayside notch locations, while red symbols are for the nightside.